DESCRIPTION OF FIBRE DISTRIBUTION WITHIN DISCONTINUOUS-FIBRE REINFORCED THERMOPLASTIC COMPOSITES USING 3D FIBRE CELLS

Y. Zhou[1,2] and P. Hubert[1,2]

[1] Structures and Composite Materials Laboratory, McGill University, Montréal, Canada
[2] Centre de recherche sur les systèmes polymères et composites à haute performance (CREPEC)

Keywords: Fibre structure characterization, Feature-property relationships, Contrastive learning.

ABSTRACT

Currently, the fibre distribution within discontinuous-fibre reinforced polymer matrix composites (DFR PMCs) is commonly described separately by different fibre distribution features such as fibre orientations and fibre lengths, while the fibre packing states and the links between different fibre distribution features are rarely addressed. The fibre-cell-based fibre distribution description framework was recently proposed for the characterization of 2D fibre domains, which is able to include both the fibre packing states and the links between different fibre distribution features into the fibre distribution description. In this study, the fibre-cell-based fibre distribution description is extended for 3D fibre domains. The relationships between the fibre distributions described by the fibre-cell-based method and their corresponding homogenized elastic modulus are obtained using an artificial neural network (ANN). Then, the ANN model is integrated with an image analysis software to provide instant predictions of elastic modulus at different locations within a DFR PMC based on its micro computed tomography (micro-CT) images. Finally, the local elastic modulus predicted by the ANN model are compared with the local elastic modulus obtained by the micro-indentation tests. It was found that the variations of elastic modulus at different locations were accurately predicted by the ANN model. Lastly, the fibre-cell-based fibre distribution description is a very versatile framework that can be easily adopted for the characterization of microstructures with different inclusion shapes at various length scales.

1 INTRODUCTION

In recent years, discontinuous-fibre reinforced polymer matrix composites (DFR PMCs) are increasingly used in the automotive industry to achieve lightweight vehicle designs. Their mechanical properties are strongly influenced by the fibre distribution within the materials. Multiscale finite element analysis (FEA) is commonly used to compute the mechanical properties of DFR PMCs: the homogenized material properties are acquired based on the fibre distribution at different locations within the material using representative volume elements (RVEs), and then the material properties can be analyzed at the component level using the material properties obtained at the local level. Homogenized material properties of RVEs are usually computed by FEA, and their computational cost are extremely high. In order to reduce the computational cost, surrogate models are often developed based on a RVE database that contains RVEs with known homogenized material properties. The surrogate models predict the homogenized material properties of a given RVE based on the similarities in the fibre distributions between the given RVE and the RVEs from the database [1,2]. The RVE fibre distributions are often quantitatively compared based on the fibre distribution features; therefore, an accurate presentation of the fibre distribution features is key to the performance of the surrogate models. Currently, the fibre distribution within the DFR PMCs is commonly described separately by different fibre distribution features such as fibre orientations and fibre lengths. However, as illustrated in Fig. 1, the fibre packing states and the links between different fibre distribution features are rarely addressed. The fibre-cell-based fibre distribution description method was recently proposed to characterize the fibre distribution within 2D domains [3]. With the new description approach, the fibre packing state of each fibre within a 2D domain can be included and the links between different fibre distribution features can also be addressed. In this study, the fibre-cell-based fibre distribution description is extended for 3D fibre domains. The fibre distribution characterized by the fibre-cell-based method is correlated to its

corresponding homogenized elastic modulus using an ANN. Then, the ANN model is integrated with an image analysis software to provide instant elastic modulus predictions based on the micro-CT images of a DFR PMC. Finally, the elastic modulus predicted by the ANN model are compared with the local elastic modulus measured by micro-indentation tests.

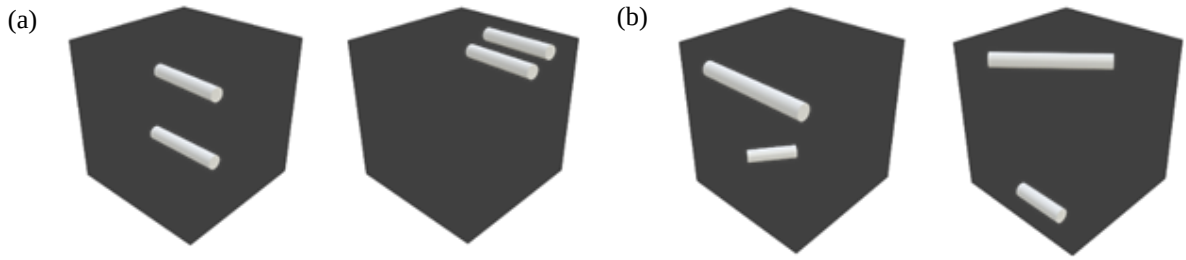

Figure 1: Fibre layouts with identical fibre length and orientation distribution but (a) different fibre packing states; (b) different links between fibre length and fibre orientation.

2 MATERIAL PROPERTY PREDICTION FRAMEWORK

2.1 Fibre Cell

A schematic of the fibre-cell-based material property prediction framework is provided in Fig. 2. Fibre cells are constructed within a fibre domain based on the location of each fibre using Voronoi diagram [4]. Consequently, the distribution features of each fibre can be represented by the properties of its fibre cell. For example, a fibre will have a slenderer cell when it is closely packed in its longitudinal direction and a rounder cell when it is loosely packed by neighbouring fibres. The fibre cell properties are parameterized by six dimensionless parameters: the local volume fraction and five shape parameters. As illustrated in Fig. 3, the local volume fraction, $x_{local\,VF}$, of the fibre cell is defined as

$$x_{local\,VF} = \frac{Volume_{fibre}}{Volume_{fibre\,cell}}. \tag{1}$$

The five shape parameters $x_{shape\,1}$~$x_{shape\,5}$, are generated based on the shape of the fibre cell using a convolutional neural network (CNN) encoder trained by contrastive learning [5]. The fibre cells are transformed into 3D images and then parameterized using the CNN encoder. The shape parameters will have the same values if the fibre cells have an identical shape, while the differences between the shape parameters will increase as the shapes of the fibre cells become more different. In this way, the shape of the fibre cells can be compared quantitatively. Then, weights are applied to the fibre cell parameters, and the fibre cells are clustered into different types based on their weighted parameters using k-means clustering algorithm [6]. As a result, the fibre distribution within a fibre domain can be described by the distribution of the fibre cell types.

2.2 Artificial Neural Network

The relationships between the fibre distribution features and their corresponding homogenized elastic modulus are established using an ANN which is trained using a RVE database that contains cubic RVEs of different fibre distributions with a side length of 100 μm. Specifically, a training set that contains 4600 RVEs is used to train the ANN model, and the performance of the ANN model is later evaluated using an independent test set that contains 300 RVEs. The homogenized elastic modulus of the RVEs along direction 1, E_{11}, as shown in Fig. 2, are obtained using the FEA framework developed by Omairey et al. with the surface mesh interpolation method proposed by Nguyen et al. to impose the periodic boundary conditions [7,8]. The ANN was signed with four layers as shown in Fig. 2. The first layer is an input layer with the number of neurons equals to the number of fibre cell types (k=100), which is assigned with the density of each fibre cell type. The second layer contains 25 neurons with 24 hidden neurons and one input neuron that contains the volume fraction of the RVE. The third layer contains 10

hidden neurons, and the fourth layer contains the output neuron which provides the prediction of the homogenized elastic modulus.

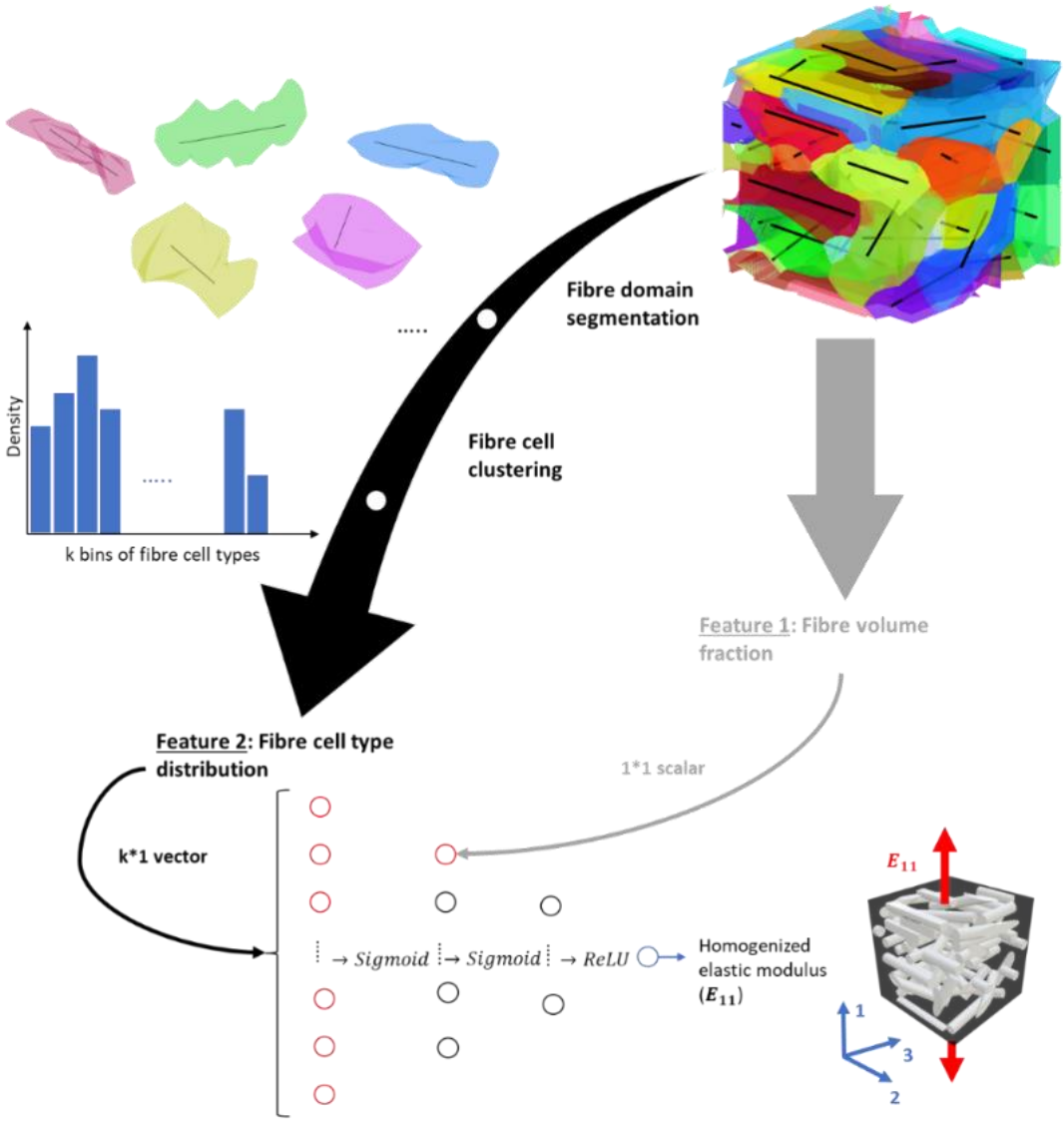

Figure 2: Homogenized elastic modulus prediction framework based on fibre-cell-based fibre distribution description.

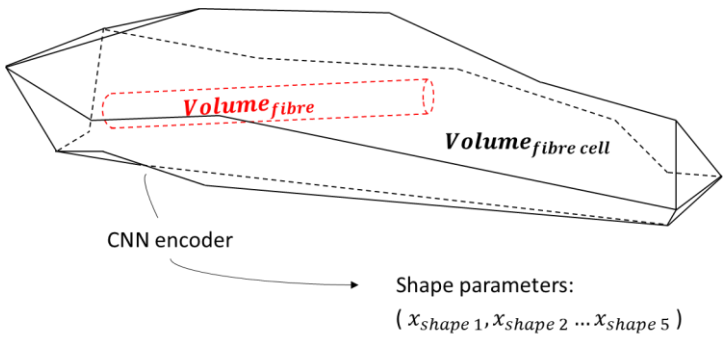

Figure 3: Definition of fibre cell parameters.

3 EXPERIMENTS

3.1 Sample Preparation

The samples used in this study were manufactured by injection moulding, with ForTii U12S PPA-I pellets from DSM mixed with 30wt.% recycled carbon fibres. The elastic modulus of the matrix and the fibre are 2.8 GPa and 255 GPa, respectively [9]. As shown in Fig. 4 (a), ASTM D-638 standard type I test specimens were injection moulded, and the elastic modulus of the work material was measured to be 14.56 GPa with a standard deviation of 0.51 GPa from tensile testing [10]. In addition, an ASTM D-638 type V specimen was cut out from the gauge section of an ASTM D-638 type I specimen, and the thickness of the ASTM D-638 type V specimen was polished to 1mm. Finally, the ASTM D-638 type V specimen was cut from the middle and mounted in a resin block with the cross-section surface polished with 0.3 µm suspensions.

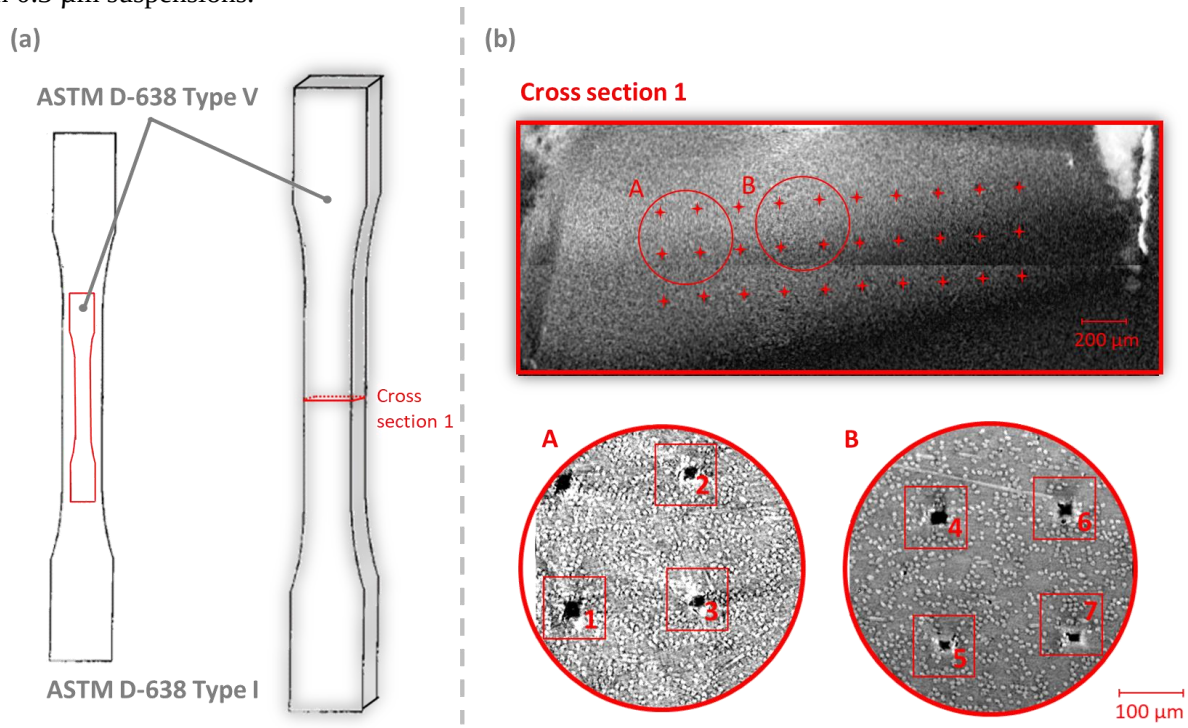

Figure 4: (a) Sample preparation process; (b) micro-indentation locations from low-resolution micro-CT scan (top) and high-resolution micro-CT scan (bottom).

3.2 Micro-indentation

Micro-indentation tests were conducted to measure the elastic modulus at different locations on the cross section. The elastic modulus at each indentation point is calculated based on the initial unloading contact stiffness using the method developed by Oliver and Pharr [11]. The elastic modulus at the vertices of a 10*3 grid with 200 µm space was measured using a Vickers diamond indenter (Anton Paar MCT3), as illustrated in Fig. 4 (b). The micro-indentation test was performed using displacement control with indentation depth of 11 µm and loading rate of 22 µm/min, which creates a square-shaped indent area with a side length of 54.45 µm. The indentation depth is selected to result in a subsurface stress zone (Von Mises stress ≥ 5% maximum contact pressure) of a similar size as the size of RVEs in the database [12].

3.3 Micro-CT Imaging

The specimen was cut out from the resin block after the micro-indentation test, and the fibre distributions at seven indentation locations were obtained using a micro-CT (ZEISS Xradia 510 Versa). A low-resolution scan (5 µm resolution) was made first on the cross section of the specimen to obtain the locations of the indents as shown in Fig. 4 (b). Then, two high-resolution scans (0.48 µm resolution)

were conducted to obtain the fibre distributions at indent 1 to 7. Subsequently, as shown in Fig. 5, cubic areas, with a side length of 96 µm, underneath the indents were cropped from the high-resolution scans. Finally, the fibre distributions within the cubes are extracted using Avizo 3D [13]. Fibre cells are then constructed within the extracted fibre domains, and the elastic modulus of the fibre domains are predicted using the ANN.

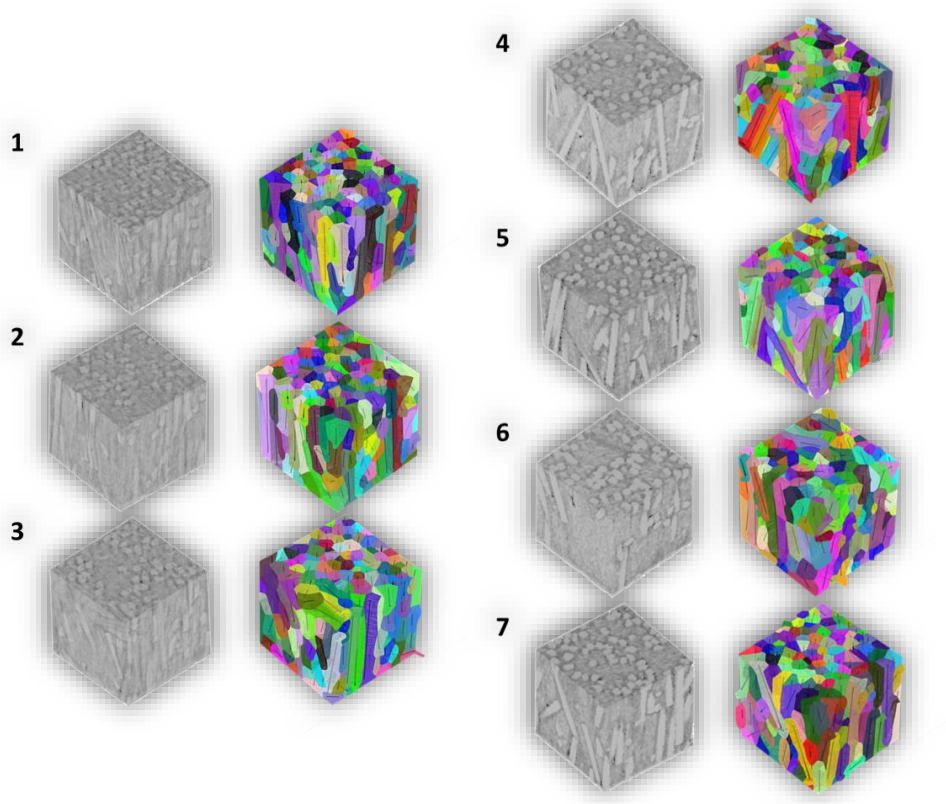

Figure 5: Fibre cells within the fibre domains under the indentation points.

4 RESULTS AND DISCUSSION

The homogenized elastic modulus predicted by the ANN model, for the RVEs in the test set, are compared with their homogenized elastic modulus computed using FEA in Fig. 6. The ideal correlation line is marked in red, and all the predictions should locate on the line if the prediction model was perfect. From the plot, it can be observed that the predictions converge to the ideal correlation line very well. Moreover, the performance of the ANN model is quantitatively evaluated by its mean absolute relative error (MARE) which is calculated as

$$MARE = \frac{1}{n}\sum_{i=1}^{n}\frac{\left|E_{11_{ANN_i}} - E_{11_{FEA_i}}\right|}{\left|E_{11_{FEA_i}}\right|}, \tag{2}$$

whereas $E_{11_{FEA_i}}$ is the homogenized elastic modulus computed by FEA, $E_{11_{ANN_i}}$ is the homogenized elastic modulus predicted by the ANN model, and n is the number of samples within the test set. The MARE is calculated to be 4.8% for the ANN model which is very close to the MARE of the ANN model from the 2D study (4.6%) [3]. Therefore, it can be concluded that the concept of fibre cell can be extended to 3D fibre domains and maintain a high accuracy in fibre distribution description despite the more complex fibre distribution states resulting from the higher dimensionality.

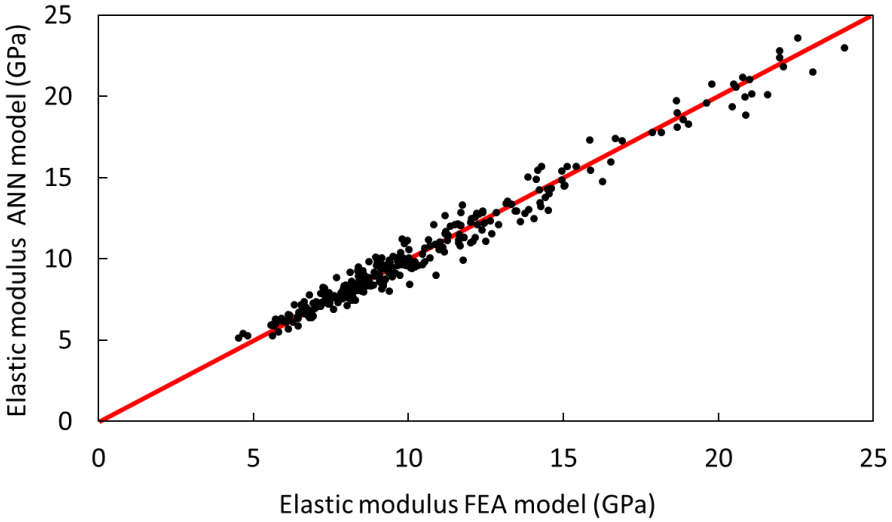

Figure 6: Homogenized elastic modulus from ANN model versus FEA model.

In Fig. 7, elastic modulus predicted by the ANN model are plotted with the elastic modulus measured by the micro-indentation test at points 1 to 7. In addition, the elastic modulus measured by the tensile test and the predicted errors of the ANN model are also shown in the figure. The plot shows a good agreement, between the elastic modulus predicted by the ANN model and measured by the micro-indentation test with an average prediction error of 5.4%. More importantly, it can be observed that the local elastic modulus measured by the micro-indentation test are fluctuating around the nominal elastic modulus obtained by tensile testing due to different fibre distributions at different indentation points, and the variations of the local elastic modulus are accurately captured by the ANN model.

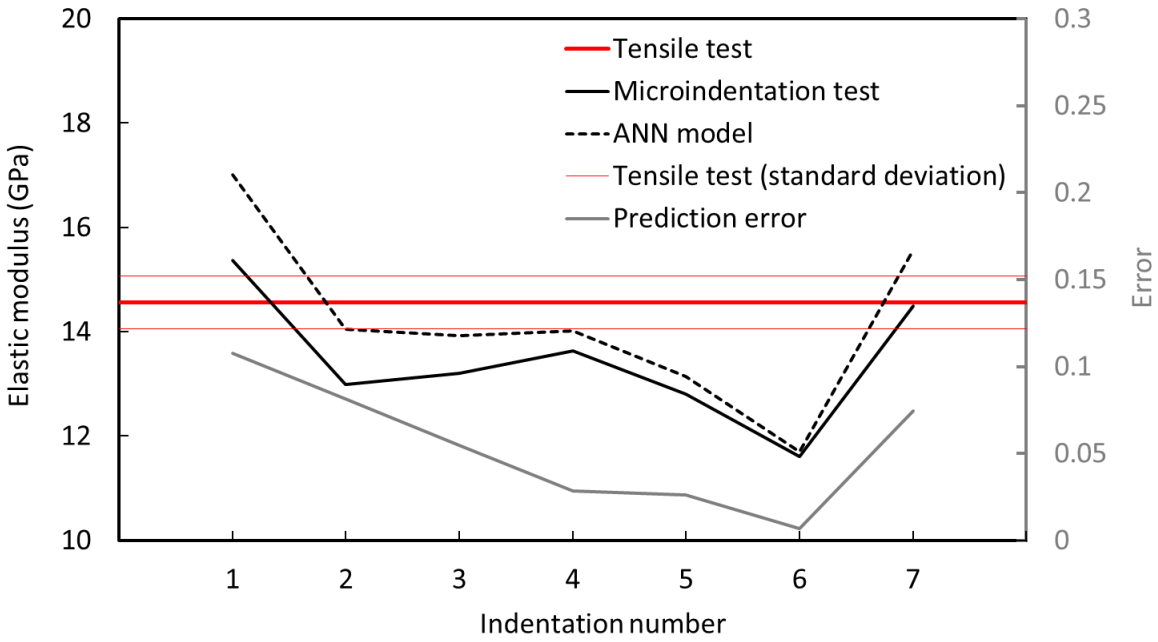

Figure 7: Comparison between the elastic modulus measured by micro-indentation tests and the ANN model.

5 CONCLUSION

In this study, a new fibre distribution description method based on the concept of fibre cell is proposed. Compared with current fibre distribution description methods, the proposed method is able to include fibre packing states and the links between different fibre distribution features in addition to the fibre distribution features that are usually considered such as the fibre orientations and lengths. Then, a surrogate model is developed based on the fibre-cell-based fibre distribution description to provide fast homogenized elastic modulus predictions using an ANN. Accurate feature-property relationships are established using the fibre-cell-based fibre distribution description thanks to its ability to include more complete fibre distribution features. Finally, the ANN model is integrated with an image analysis software to provide instant local elastic modulus predictions based on the micro-CT images of a DFR PMC. The elastic modulus predicted by the ANN are compared with the local elastic modulus measured by micro-indentation tests. The ANN predicted elastic modulus show a good agreement with the experimental data, and the variations of the local elastic modulus with in the DFR PMC are accurately captured by the ANN model. As the results have shown, the fibre-cell-based fibre distribution description can be integrated into image analysis tools to provide fast local elastic modulus predictions with an ANN without the need of running any additional laboratory tests or numerical simulations. Lastly, as all fibre cell parameters are dimensionless, the fibre-cell-based fibre distribution description is also a very versatile framework that can be adopted for microstructure characterizations in different scales and with inclusions of different shapes.

ACKNOWLEDGEMENTS

The authors acknowledge the funding from the Natural Sciences and Engineering Research Council (NSERC), Canada, the Ford Motor Company, the Research Center for High Performance Polymer and Composite Systems (CREPEC), Canada, and the McGill Engineering Doctoral Awards (MEDA), Canada. We also would like to thank Digital Research Alliance of Canada for providing the computational resources, Bruno Noronha Castilho from McGill Surface Engineering and Coating Tribology Laboratory for micro-indentation testing, Marie-Hélène Bernier from Montreal Polytechnic Microfabrication Lab for micro-CT scanning, and Professor Mohini Sain from University of Toronto for providing the tensile testing data.

REFERENCES

[1] J. Köbler, M. Schneider, F. Ospald et al., Fiber orientation interpolation for the multiscale analysis of short fiber reinforced composite parts. *Computational Mechanics*, 61, 2018, pp 729–750 (doi: https://doi.org/10.1007/s00466-017-1478-0)

[2] C. Rao, Y. Liu, Three-dimensional convolutional neural network (3D-CNN) for heterogeneous material homogenization, *Computational Materials Science*, 184, 2020, pp 109850 (doi: https://doi.org/10.1016/j.commatsci.2020.109850)

[3] Y. Zhou and P. Hubert, Properties prediction of discontinuous-fibre reinforced thermoplastic composites with fibre-cell-based fibre distribution description. *Materials Today Communications*, Vol. 33, 2022, pp 10456 (doi: https://doi.org/10.1016/j.mtcomm.2022.104565).

[4] F. Aurenhammer and R. Klein, *Voronoi Diagrams*, Handbook of Computational Geometry, North-Holland, 2000

[5] L. Sorensen, T. Gmür and J. Botsis, Delamination propagation measurement using long gauge-length FBG sensors, *Proceedings of the 3rd International Conference on Composites Testing and Model Identification CompTest 2006 (Eds. P. Camanho, F. Pierron, M. Wisnom), Porto, Portugal, April 10-12, 2006*, University Press, Porto, Paper 41, 2006, pp. 174-175.

[6] J. A. Hartigan, and M. A. Wong, Algorithm AS 136: A K-Means Clustering Algorithm. *Journal of the Royal Statistical Society. Series C (Applied Statistics)*. 28, no.1, 1979, pp 100–108 (doi: https://doi.org/10.2307/2346830).

[7] S.L. Omairey, P.D. Dunning, and S. Sriramula, Development of an ABAQUS plugin tool for periodic RVE homogenisation. *Engineering with Computers*, 35, 2019, pp 567–577 (doi: https://doi.org/10.1007/s00366-018-0616-4)

[8] V.-D. Nguyen, E. Béchet, C. Geuzaine, L. Noels, Imposing periodic boundary condition on arbitrary meshes by polynomial interpolation. Computational Materials Science, Volume 55, 2012, pp 390-406, (doi: https://doi.org/10.1016/j.commatsci.2011.10.017)

[9] B. S. Maia, J. Tjong and M. Sain, Material characterization of recycled and virgin carbon fibers for transportation composites lightweighting. *Materials Today Sustainability*, Vol. 5, 2019, pp 100011 (doi: https://doi.org/10.1016/j.mtsust.2019.100011).

[10] Test Method for Tensile Properties of Plastics. *ASTM International*, (doi: https://doi.org/10.1520/d0638-14)

[11] W.C. Oliver, G.M. Pharr, An improved technique for determining hardness and elastic modulus using load and displacement sensing indentation experiments. *Journal of Materials Research*, 7, 1992, pp 1564–1583, (doi: https://doi.org/10.1557/JMR.1992.1564).

[12] Q.J Wang, D. Zhu, *Hertz Theory: Contact of Spherical Surfaces*, Encyclopedia of Tribology. Springer, Boston, MA. (doi: https://doi.org/10.1007/978-0-387-92897-5_492)

[13] Thermo Fisher Scientific. (2021). Avizo3D [Computer software], https://www.thermofisher.com/